HHS Public Access

Author manuscript

J Mol Cell Cardiol. Author manuscript; available in PMC 2018 November 01.

Published in final edited form as:

J Mol Cell Cardiol. 2017 November ; 112: 104–113. doi:10.1016/j.yjmcc.2017.09.007.

Endothelial Specific SIRT3 Deletion Impairs Glycolysis and Angiogenesis and Causes Diastolic Dysfunction

Xiaochen He, MS[1], **Heng Zeng, MD**[1], **Sean T Chen, BS**[2], **Richard J Roman, PhD**[1], **Judy L Aschner, MD**[3], **Sean Didion, PhD**[1], and **Jian-Xiong Chen, MD**[1]

[1]Department of Pharmacology and Toxicology, University of Mississippi Medical Center Jackson, MS, USA

[2]Duke University School of Medicine, Durham, NC

[3]Department of Pediatrics, Albert Einstein College of Medicine and the Children's Hospital at Montefiore, Bronx, NY

Abstract

Endothelial glycolysis plays a critical role in the regulation of angiogenesis. We investigated the role of Sirtuin 3 (SIRT3) on endothelial cell (EC) glycolytic metabolism, angiogenesis, and diastolic function. Our aim was to test the hypothesis that loss of SIRT3 in ECs impairs endothelial glycolytic metabolism and angiogenesis and contributes to myocardial capillary rarefaction and the development of diastolic dysfunction. Using SIRT3 deficient ECs, SIRT3 was found to regulate a metabolic switch between mitochondrial respiration and glycolysis. SIRT3 knockout (KO)-ECs exhibited higher mitochondrial respiration and reactive oxygen species (ROS) formation. SIRT3 knockout (KO)-ECs exhibited a reduction in the expression of glycolytic enzyme, PFKFB3, and a fall in glycolysis and angiogenesis. Blockade of PFKFB3 reduced glycolysis and downregulated expression of VEGF and Angiopoietin-1 (Ang-1) in ECs. Deletion of SIRT3 in ECs also impaired hypoxia-induced expression of HIF-2α, VEGF, and Ang-1, as well as reduced angiogenesis. *In vivo*, endothelial-specific SIRT3 KO (ECKO) mice exhibited a myocardial capillary rarefaction together with a reduced coronary flow reserve (CFR) and diastolic dysfunction. Histologic study further demonstrated that knockout of SIRT3 in ECs significantly increased perivascular fibrosis in the coronary artery. These results implicate a role of SIRT3 in modulating endothelial function and cardiac function. Ablation of SIRT3 leads to impairment of EC glycolytic metabolism and angiogenic signaling, which may contribute to coronary microvascular rarefaction and diastolic dysfunction in SIRT3 ECKO mice.

Address for Correspondence: Jian-Xiong Chen, M.D., Department of Pharmacology and Toxicology, University of Mississippi Medical Center, 2500 North State Street, Jackson, MS, 39216, Office: 601-984-1731, Fax: 601-984-1637, JChen3@umc.edu.

Supplementary Material

Supplementary data to this article can be found online at *Journal of Molecular and Cellular Cardiology*.

Disclosures

The authors declare no conflict of interest.

Keywords

SIRT3; PFKFB3; metabolic reprogram; coronary microvascular dysfunction; diastolic dysfunction

Subject Codes

Coronary Circulation; Epigenetics; Echocardiography; Heart Failure; Metabolism

1. Introduction

Heart failure (HF) is a high prevalent, progressive disease that develops with advanced age, hypertension, and diabetes [1–4]. Heart failure is typically divided into two phenotypes, heart failure with reduced ejection fraction (HFrEF) and heart failure with preserved ejection fraction (HFpEF). More than half of newly diagnosed heart failure patients present with preserved ejection fraction [5, 6]. Standard of care medications for HFrEF have long been established, but thus far, large clinical trials have failed to show any significant benefit in life expectancy in patients with HFpEF [7]. Despite the clinical importance of HFpEF, our understanding of its pathophysiology and molecular mechanism is incomplete.

Endothelial (EC) dysfunction is highly prevalent in HFpEF patients and is correlated with exercise intolerance [8, 9]. A recent clinic study indicates that microvascular rarefaction is a major contributor to diastolic dysfunction in HFpEF patients [3]. SIRT3 is predominately localized in the mitochondria of the heart, has emerged as a novel regulator of mitochondrial function and cellular metabolism [4, 10, 11]. SIRT3 levels were decreased as much as 40% in elderly adults with sedentary lifestyles compared to younger individuals [12]. Our recent study indicated that a fall in SIRT3 levels is associated with obesity-induced microvascular rarefaction and cardiac dysfunction [13]. Gene therapy with the angiogenic growth factor, apelin, increased myocardial vascular density and attenuated ischemia-induced cardiac dysfunction in diabetic STZ mice, but had no effect in STZ-SIRT3 knockout (KO) mice [14]. These studies indicate that loss of SIRT3 contributes to development of heart failure. Endothelial metabolism plays a critical role in the regulation of angiogenesis since ECs depend on glycolysis for migration and proliferation [15, 16]. The 6-phosphofructo-2-kinase/fructose-2, 6-bisphosphatase, isoform 3 (PFKFB3) is a key regulator of glycolysis in endothelial cells (EC), that has been shown to promote angiogenic sprouting [15, 17, 18]. Our recent study demonstrated a significant reduction of PFKFB3 expression and impaired angiogenesis in the heart of SIRT3 KO mice [19]. However, a direct role of SIRT3 in endothelial glycolytic metabolism, angiogenesis and diastolic function is unknown and has not been studied previously.

We hypothesized that endothelial SIRT3 regulates the glycolytic metabolism for maintaining coronary microvascular function and diastolic function. In the absence of SIRT3, the glycolytic metabolism of EC is reduced, which contributes to impairment of angiogenesis and coronary microvascular dysfunction and diastolic dysfunction. To test this hypothesis, we investigated the cardiac phenotype of endothelial-specific SIRT3 knockout (SIRT3 ECKO) mice and examined endothelial glycolytic metabolic profiles in SIRT3 KO-ECs.

2. Materials and Methods

2.1. Chemicals and Reagents

Dimethyl sulfoxide (DMSO) were from Sigma-Aldrich (MO, USA). Geltrex® LDEV-free reduced growth factor basement membrane matrix (ECM) was from Invitrogen (Life Technologies, NY). L-glutamine (200 mM) and sodium pyruvate (100 mM) were from GIBCO (Invitrogen, Life Technologies, NY). 3-(3-Pyridinyl)-1-(4-pyridinyl)-2-propen-1-one (3PO) was from EMD Millipore (MA, USA). Dihydroethidium (DHE) was from Molecular Probes (OR, USA).

2.2. Animals

All animals were fed with laboratory standard chow and water, and housed in individually ventilated cages in the Laboratory Animal Facilities at the University of Mississippi Medical Center. All protocols were approved by the Institutional Animal Care and Use Committee (IACUC) of the University of Mississippi Medical Center (Protocol ID: 1280B) and were consistent with the National Institutes of Health Guide for the Care and Use of Laboratory Animals (NIH Pub. No. 85-23, Revised 1996).

2.3. Generation of SIRT3 ECKO Mice

SIRT3 ECKO mice were generated using the Cre -LoxP system as depicted in Figure S1A. $SIRT3^{flox/flox}$ mice were originally obtained from Dr. Eric Verdin at Gladstone Institute of Virology and Immunology, University of California. The exons 2 and 3 of SIRT3 gene are flanked with LoxP sites, priming for subsequent deletion by Cre recombinase. $SIRT3^{flox/flox}$ mice were crossbred with VE-Cadherin-Cre (Cdh5-Cre) transgenic mice [B6.FVB-Tg(Cdh5-cre)7Mlia/J from Jackson Laboratories] expressing Cre recombinase in vascular endothelial cells (Figure S1A). The resulting Cdh5-Cre/$SIRT3^{flox/-}$ heterozygous mutants were then mated with $SIRT3^{flox/flox}$ to obtain endothelial-specific ablated SIRT3 mutant mice (SIRT3 ECKO). Only male mice (12 month of age) were used for all the experiments and $SIRT3^{flox/flox}$ (SIRT3 LoxP) mice were used as the corresponding control. Genotyping was performed by tail DNA PCR analysis. Primer sequences used for genotyping floxed SIRT3 allele were as follows: SIRT3 Forward 5′-TACTGAATATCAGTGGGAACG-3′, SIRT3 Reverse 5′-TGCAACAAGGCTTTATCTTCC-3′, and SIRT3 WT Forward 5′-CTTCTG CGGCTCTATACACAG-3′. Cdh5-Cre transgene was detected using the following primers: transgene forward 5′-GCGGTCTGGCA GTAAAAACTATC-3′ and transgene reverse 5′-GTGAAACAGCATTGCTGTCACTT-3′; internal positive control forward 5′-CTAGGCCAC AGAATTGAAAGATCT-3′ and internal positive control reverse 5′-GTAGGTGGAAATTCT AGCATCATCC-3′. PCR products were analyzed on 1.5% tris-acetate-EDTA (TAE) agarose gels (Figure S1B and S1C). To confirm that SIRT3 was knocked out at protein level, the isolated endothelial cells from SIRT3 LoxP and SIRT3 ECKO mice were co-stained with rabbit anti-SIRT3 antibody (ab86671, Abcam, MA) and Alexa Fluor® 488 conjugated *Griffonia Bandeiraea Simplicifolia* Isolectin B4 (1:50; IB4, Invitrogen, OR), followed by incubation with anti-rabbit Cy™3 conjugated secondary antibody (Jackson ImmunoResearch Inc, PA). Pictures were taken using a Nikon Eclipse 80i microscope, coupled with an X-Cite® 120 Fluorescence Illumination system (Nikon Instruments, NY). The absence of SIRT3 was also confirmed by immunoblot analysis.

2.4. Echocardiography

Transthoracic echocardiograms were performed on SIRT3 LoxP and SIRT3 ECKO using a Vevo770 High-Resolution In Vivo Micro-Imaging System equipped with a RMV 710B scanhead (VisualSonics Inc, Canada). The studied mouse was anesthetized by inhalation of 1.5–2% isoflurane mixed with 100% medical oxygen administered with a vaporizer in an isolated chamber for induction. Anesthesia was maintained with 1–1.5% isoflurane with a heart rate of ~400–450 beats per min (bpm).

For LV diastolic function, transmitral inflow Doppler images are obtained in apical 4-chamber (A4C) view using pulsed-wave (PW) Doppler mode to measure the ratio of peak velocity of early to late filling of mitral inflow (E/A), isovolumic relaxation time (IVRT), isovolumic contraction time (IVCT) and ejection time (ET) [20]. The myocardial performance index (MPI), is calculated as the following formula: MPI = (IVRT + IVCT)/ET. In addition, Tissue Doppler images are obtained from the mitral annulus to measure tissue motion velocity in early and late diastole (E′ and A′, respectively).

For coronary flow reserve, the left proximal coronary artery (LCA) is visualized in a modified parasternal LV short-axis view, and cine loop of LCA is recorded at baseline, and under hyperemic conditions induced by inhalation of 1% and 2.5% isoflurane, respectively. The coronary flow reserve (CFR) is calculated as the ratio of hyperemic peak diastolic flow velocity to baseline peak diastolic flow velocity [19, 21].

2.5. Primary EC Culture and Treatment

Microvascular endothelial cells (MECs) were isolated from WT or SIRT3 KO mice (n=3) as described previously [22]. In brief, The WT and SIRT3 KO mice were anesthetized with ketamine (100 mg/kg) and xylazine (15 mg/kg). The lung was perfused with 10 ml chilled PBS containing 2.5 mM EDTA, followed by perfusion of 5 ml of chilled 0.25% trypsin/2 mM EDTA through the right ventricle of the heart. The heart and lung were then removed *en bloc* and incubated at 37 °C for 20 min. Small cuts were made in the visceral plura and the ECs can be harvested by pipetting 1.5 ml EGM-2 medium (Lonza, MD) supplemented with growth factors and 10% fetal bovine serum (FBS) up and down 10–15 times. The cell suspension was filtered through a 100 μm filter and plated into 60 mm cell culture dish. After 3 days of incubation, ECs formed small colonies and non-ECs were removed by vacuum until >90% ECs left. Purity of these cells was checked by staining with rabbit anti-von Willebrand factor (vWF) polyclonal antibody (Santa Cruz biotechnology, TX) (Figure S2A). The absence of the expression of SIRT3 protein was confirmed in three independent EC lines (Figure S2B). ECs were cultured in EGM-2 medium at 37 °C with 5% CO_2. Cells between passage 4 and 10 were used for all the studies. ECs were used for metabolic evaluation and tube formation assay in the presence or absence of 3-(3-Pyridinyl)-1-(4-pyridinyl)-2-propen-1-one (3PO) (5–15 μM) [23].

For hypoxia studies [24], the cells were exposed to normoxia (PO_2 = 160 mmHg) or hypoxia (PO_2 < 10 mmHg) for various time periods with basic medium containing 0.1% FBS in normal incubator or an air-tight chamber (MIC-101, Billups-Rothenberg, Inc.) flushed with 95% N_2/5% CO_2. The cells were then immediately harvested for western blot analysis.

2.6. Metabolic Assays

Glycolysis and mitochondrial function was determined using XF^{e}24 extracellular flux analyzer from Seahorse Bioscience, following the manufacturer's instructions. Briefly, cells were seeded in TC-treated 24-well plate (V7-PS) at the density of 25000 cells per well as determined by a pilot cell density assay. The next day, the attached cells were treated in the presence or absence of 3PO (5–15 μM) for the time as indicated in the text [23]. Control group was treated with vehicle (DMSO). After treatment, the cells were incubated in unbuffered assay medium supplemented with various substrates as described below, at 37 °C in a non-CO_2 incubator for one hour prior to analysis. For the glycolysis stress test, the unbuffered assay medium was supplemented with glutamine (2mM) only. The baseline of ECAR was measured, followed by the sequential injection of the following compounds with indicated final concentration: glucose (10 mM), oligomycin (1 μM), and 2-deoxyglucose (2-DG, 100 mM). For cellular mitochondrial stress test, the unbuffered assay medium was supplemented with glucose (10 mM), pyruvate (1 mM) and glutamine (2 mM). The baseline of OCR was measured, followed by the sequential injection of the following inhibitors with indicated final concentration: oligomycin (1 μM), cyanide p-trifluoromethoxy-phenylhydrazone (FCCP, 1 μM) and rotenone/antimycin A (0.5 μM). Basal glycolysis and glycolytic capacity were calculated from the raw data using Seahorse report generator.

2.7. Wound Scratch Migration Assay

Wound scratch migration assays were performed as previously described [25]. Briefly, 2×10^5 cells per well were seeded in a 24-well plate. A scratch wound was applied on confluent ECs monolayer using a 10 μL pipette tip, and then photos were taken as T0 using an AMG inverted phase-contrast microscope (AMG, Life Technologies, NY). The cultures were further incubated for 12 hours and photographed again (T12). Migration distance (the average of three measurements of gap distance at T0 minus the average of three measurements of gap distances at T12 and then divided by two) was measured with NIH Image J software and is expressed in μm.

2.8. Tube Formation Assay

Tube formation assay was performed as previously described with minor modifications [26]. Briefly, ECs were harvested after indicated treatments and then seeded into a 96-well plate (2×10^4 cells/well) pre-coated with 40 μL reduced-growth factor ECM. After 6 hours of incubation at 37 °C with 5% CO_2, the capillary tube structures were observed and representative images were captured with an AMG inverted phase-contrast microscope (AMG, Life Technologies, NY). The total branching length was quantified by NIH Image J software with angiogenesis analyzer plug-in (developed by Gilles Carpentier, http://image.bio.methods.free.fr/ImageJ/?Angiogenesis-Analyzer-for-ImageJ).

2.9. Mouse Aortic Ring Sprouting Assay

Ex vivo angiogenesis was evaluated by using isolated mouse aortas. Aortic explants were prepared for sprouting assay as our described previously [27–30]. Briefly, one aortic ring was placed in a well of a 96-well culture plate covered with total of 80 μL of ECM gel. Vessel outgrowth was examined on day 7 using an inverted microscope. Quantification of

vessel sprouting was performed by measuring the relative area of aortic explants outgrowth using image software (Image J, NIH).

2.10. Reactive Oxygen Species Formation

Superoxide formation was measured and quantified by staining with DHE [31]. Briefly, the ECs were seed on an 8-well chamber slide at density of 2×10^4 cells/well and washed with PBS to remove any embed compound. The slides were then incubated with DHE at the concentration of 2–5 μM at 37 °C for 30 min in dark. Excessive DHE was washed off with PBS twice. Immediately after mounting, images were captured using a fluorescent microscope at excitation and emission wavelengths of 520 and 610 nm, respectively. The results are presented as normalized ROS levels derived from total fluorescence intensity per field relative to the area measured.

2.11. Histology and Immunofluorescence

Paraffin-embedded left ventricles were prepared and cut to make 5-μm cross sections. Microscopic photos of 5 to 10 fields per section were taken using a Nikon Eclipse 80i microscope (Nikon Instruments, NY). In each representative slide, trichrome staining around coronary arteries was semi-automatically quantified by the Image J software (Image J, NIH), expressed as perivascular fibrosis index using the following formula: perivascular fibrosis index (μm) = perivascular area (μm^2)/vessel outer perimeter (μm). The results from all fields were averaged.

Cryostat sections (10) μm of the ventricles were stained with Alexa Fluor® 488 conjugated IB4 (Invitrogen, OR) to visualize capillaries. Microscopic photos were taken using a Nikon Eclipse 80i microscope.

2.12. Immunoblot Analysis

Protein extractions from heart ventricular samples or cultured ECs were prepared in lysis buffer with protease inhibitor cocktail. Lysates were separated by SDS-PAGE under reducing conditions, transferred to a PVDF membrane, and analyzed by immunoblotting. The PVDF membranes were probed with antibodies specific to SIRT3 (5490), GAPDH (2118) (Cell Signaling Technology, MA), HIF -2α (NB100–122, Novus Biologicals, CO), PFKFB3 (ab181861, Abcam, MA), Angiogpoietin-1 (A0604, Sigma-Aldrich, MO), or VEGF (sc-507, Santa Cruz Biotechnology, TX). The membranes were then washed and incubated with an anti-rabbit or anti-mouse secondary antibody conjugated with horseradish peroxidase. Densitometries were analyzed using TINA 2.0 image analysis software.

2.13. Statistical Analysis

Data are presented as mean ± SEM. Statistical significance was determined using a Student's *t*-test (two-tailed) between means of two groups, or one -way ANOVA, followed by Tukey's *post-hoc* test (Sigmaplot v12.5). $P < 0.05$ was considered as statistically significant.

3. Results

3.1. SIRT3 deficiency is associated with decreased glycolysis in ECs

The glycolytic enzyme phosphofructokinase-2/fructose-2, 6-bisphosphatase-3 (PFKFB3) is the key regulator of endothelial glycolysis. Therefore, we investigated the expression of PFKFB3 in SIRT3 KO-ECs. Interestingly, the level of PFKFB3 was significantly reduced in SIRT3 KO-ECs (Figure 1A). Knockout of SIRT3 also increased acetylation of PFKFB3 (Figure 1B). We studied whether loss of SIRT3 affected glycolysis by measuring ECAR in WT and SIRT3 KO-ECs. Knockout of SIRT3 in ECs led to a dramatic reduction of basal glycolysis and glycolytic capacity compared to WT (Figure 1C, 1D, and Figure S3A).

We studied whether loss of SIRT3 affected mitochondrial respiration by measuring cellular oxygen consumption rate (OCR) in WT and SIRT3 KO-ECs. SIRT3 KO-ECs exhibited higher basal OCR and maximum respiratory capacity compared to WT (Figure 2A, 2B, and Figure S3B). This was accompanied by a significantly increase in ROS production (Figure 2C and 2D). To examine the effect of different substrate on the mitochondrial function, we measured OCR in the presence of pyruvate but without glucose (glycolysis) and found that basal OCR and maximum respiration capacity was also significantly higher in SIRT3 KO-ECs compared to WT-ECs (Figure 2E). These data suggest that SIRT3 deletion causes metabolic shift from oxygen-independent glycolysis to oxygen-dependent oxidative phosphorylation in ECs (Figure 2F).

3.2. Role of PFKFB3 in altering glycolysis and angiogenesis in SIRT3 KO ECs

To further determine whether blockade of PFKFB3 inhibits EC glycolysis and impairs endothelial angiogenesis, ECs were treated with the PFKFB3 inhibitor, 3PO, for 24 hours. As shown in Figure 3A, exposure of ECs to 3PO dose-dependently suppressed EC glycolysis. Moreover, treatment of ECs with 3PO decreased the expression of Ang-1 and VEGF in a dose dependent manner (Figure 3B). Inhibition of PFKFB3 resulted in a significant reduction of tuber formation (Figure 3C), suggesting that disruption of glucose metabolism leads to impaired angiogenic signaling of ECs.

3.3. Deletion of SIRT3 impairs angiogenic properties of EC and causes myocardial capillary rarefaction

We tested if the reduction of glycolysis in SIRT3 KO-ECs decreases angiogenic potential. Tube formation was reduced in SIRT3 KO-ECs (Figure 4A and 4B). Moreover, SIRT3 KO-ECs exhibited a significantly lower rate of migration than WT cells (Figure 4C and 4D). These data indicate that SIRT3 deficiency impairs angiogenic properties. In addition, *ex vivo* study of aortic rings from SIRT3 ECKO mice exhibited decreased sprouting angiogenesis relative to that from WT animals (Figure 4E and 4F). Moreover, the capillary density in the heart was significantly decreased (Figure 4G and 4H), suggest that ablation of SIRT3 causes myocardial capillary rarefaction.

3.4. Loss of SIRT3 impairs hypoxic signaling in ECs

We found that tube formation under hypoxia was less potent in SIRT3 KO-ECs than that in WT-ECs (Figure 5A and 5B). To further investigate the role of SIRT3 in altering the

expression of HIFα and the response to hypoxia, ECs were exposed to hypoxia for 6 or 24 hours. Exposure to hypoxia resulted in a gradual increase in the expression of HIF-2α in both WT and SIRT3 KO-ECs (Figure 5C). However, hypoxia-induced expression of HIF-2α was significantly less in SIRT3 KO-ECs compared to WT-ECs (Figure 5C). We also found that hypoxia-induced expression of angiopoietin-1 (Ang-1) and VEGF was increased in WT-ECs, but not in SIRT3 KO-ECs (Figure 5D and 5E).

3.5. Endothelial deletion of SIRT3 in mice reduces CFR and exhibits an HFpEF phenotype

Since SIRT3 deficiency resulted in impaired angiogenic properties of ECs and capillary rarefaction, we hypothesized that endothelial-specific SIRT3 null mice might develop microvascular dysfunction and subsequent diastolic dysfunction. To investigate the role of endothelial SIRT3 in diastolic dysfunction *in vivo*, floxed SIRT3 mice were generated and then bred with cdh5-Cre mice to create mice with SIRT3 deficiency in endothelial cells only (Figure S1). Immunostaining confirmed that SIRT3 was knocked out at protein level (Figure 6A). The absence of SIRT3 was also confirmed by immunoblot analysis (Figure 6B). Intriguingly, the protein expression of SIRT1 was significantly increased in SIRT3 ECKO ECs compared to SIRT3 LoxP ECs (Figure S4), which may be a compensatory mechanism responding to deletion of SIRT3 in ECs. Histologic study indicated that there was a significant increase in perivascular fibrosis around the coronary artery in SIRT3 ECKO mice compared to the control mice (Figure 6C and 6D).

Knockout of endothelial SIRT3 resulted in a dramatic decrease in CFR (Figure 7A and 7B). Echocardiography revealed that left ventricular dimensions were significantly increased in SIRT3 ECKO mice, indicating a dilated LV (Figure S5A and S5B). Pulse-wave (PW) Doppler measurements indicated that SIRT3 ECKO mice developed diastolic dysfunction with prolonged IVRT and increased MPI (Figure 7C and 7D). Tissue Doppler indicated that the peak velocity of E′ was significantly decreased, resulting in an increase in E/E′ ratio (Figure 7E and Table 1).

4. Discussion

This study indicates that specific ablation of SIRT3 in ECs results in an increase in oxidative phosphorylation and a reduction in glycolysis that is associated with impairment in angiogenesis. With time, these abnormalities lead to a reduction of CFR and diastolic dysfunction in mice. These results reveal a novel cell-specific effect of SIRT3 on EC glycolytic metabolism that promotes diastolic dysfunction and suggests that drugs that enhance expression of SIRT3 might be potential therapeutic targets for HFpEF.

SIRT3 is a mitochondrial deacetylase and its expression is the highest in metabolically active tissue. Using muscle- or liver-specific SIRT3 KO mice, previous study suggested non-tissue-specific roles for SIRT3 in global metabolic homeostasis [32]. However, a recent study demonstrated that SIRT3 regulates mitochondrial functions common to brain, heart, kidney, liver, and skeletal muscle, but differentially regulates metabolic pathways in fuel-producing and fuel-utilizing tissues, suggesting that SIRT3 regulates mitochondrial acetylation in a tissue -specific manner [33]. Thus, the functional role of SIRT3 is likely much more complex than initially appreciated and may involve tissue and cell specific actions. For

instance, deficiency of SIRT3 in myoblast and cancer cells decreases mitochondrial respiration and increases ROS formation [34, 35]. Moreover, respiratory capacity and ATP synthesis were decreased in cardiac mitochondria of SIRT3 deficient mice [36]. Although the mitochondrial function of SIRT3 has been investigated, the metabolic alterations associated with SIRT3 deficiency in ECs have not been examined. The present study is the first to examine the functional role of endothelial SIRT3 deficiency on glycolytic metabolism and cardiac function.

ECs have high glycolytic activity that is much higher than that of cardiomyocytes and other cell types [18]. Despite immediate access to oxygen in the blood stream, healthy ECs rely on glycolysis rather than oxidative phosphorylation to maintain proper function in response to hypoxia and nutrient deprivation [15, 37]. ECs can increase glycolytic flux in part, by upregulating the expression of PFKFB3 [15, 38]. By promoting glycolysis to generate ATP, ECs save oxygen for the adjacent cardiomyocytes and protect themselves from mitochondrial electron leakage and generation of ROS [39]. In the present study, we demonstrated that PFKFB3 was dramatically decreased in the SIRT3 KO-ECs, along with impaired glycolytic function. Loss of SIRT3 also increased oxygen consumption rate and production of ROS in ECs. These data suggest that there is a shift in metabolism and increased oxidative stress in SIRT3 KO-ECs, such that they are more dependent on oxidative phosphorylation and thus less flexible in metabolism. Most importantly, impairment of glycolysis reduces angiogenesis in SIRT3 KO ECs that may limit oxygen accessible to cardiomyocyte, which could cause cardiac hypoxia and dysfunction. Consistent with recent reports that inhibition of PFKFB3 blocks angiogenesis [15, 17, 18], our data show that PFKFB3 blockade by 3PO resulted in a reduction of glycolysis, decreased expression of angiogenic factors and angiogenesis in EC cells. These data suggest that loss of SIRT3 may induce endothelial metabolic dysfunction by reducing PFKFB3-mediated glycolysis.

Metabolic dysfunction in ECs can lead to endothelial dysfunction which limits the ability to dilate and increase blood flow in response to increased metabolic demand or ischemia. Therefore, microvascular dysfunction may contribute to chronic hypoxia in the heart. ECs are mostly quiescent but can sense and respond to signals released from surrounding hypoxic tissue, resulting in a shift to highly glycolytic metabolism [10, 40]. This phenotype change is mainly mediated through activation of HIF signaling pathway [15, 18, 41, 42]. Normal tissue reacts to hypoxia by increasing expression of angiogenic factors and promoting angiogenesis via activation of HIFα system to preserve oxygen supply and alleviate ischemia-induced injury. HIF-2α deficiency is associated with impaired homeostasis of ROS and cardiac hypertrophy that may lead to diastolic dysfunction [43]. The present study demonstrates that loss of SIRT3 impairs HIF-2α signaling and angiogenesis in EC during hypoxia and decreases capillary density in the hearts of SIRT3 ECKO mice. Microvascular rarefaction is associated with aging, diabetes, and obesity. Clinical studies of HFpEF patients suggest that abnormalities in coronary microcirculation induced by endothelial dysfunction and coronary microvascular rarefaction are associated with HFpEF [3]. Our SIRT3 ECKO mice developed coronary microvascular dysfunction as evidenced by decreased CFR. Endothelial dysfunction and decreased microvascular density is thought to limit CFR [3]. Therefore, decreased CFR in SIRT3 ECKO mice may implicate impaired myocardial perfusion. Moreover, excessive production of ROS has been shown to

diminish nitric oxide bioavailability to cardiomyocytes [44]. ROS production was dramatically elevated in SIRT3 KO-ECs, suggesting possibly impaired NO-cGMP-dependent mechanism that contributed to decreased CFR, impaired cardiomyocyte relaxation and subsequently prolonged IVRT. Taken together, these data suggest that endothelial-specific SIRT3 ablation in mice impaired coronary microvascular and diastolic function by the mechanisms involving disruption of endothelial metabolism, HIFα signaling and angiogenesis.

In conclusion, our study provides a molecular mechanism by which endothelial SIRT3 regulates endothelial function and angiogenesis by altering glycolysis and mitochondrial respiration, coronary microvascular function, and diastolic function as proposed in Figure 8. Our data suggest a cell-specific role of SIRT3 in regulation of cell metabolism and cardiac function during aging, especially in ECs. It provides a link between aging and HFpEF and suggests a potential target for therapeutic intervention.

Supplementary Material

Refer to Web version on PubMed Central for supplementary material.

Acknowledgments

This work was supported by grants from National Institutes of Health (2R01HL102042-05) and from University of Mississippi Medical Center Intramural Research Support Program to J.X. Chen. This work was partially supported by grant from National Institutes of Health (#HL-107632) to S. Didion.

We would like to thank Dr. Eric Verdin at Gladstone Institute of California for providing the original $SIRT3^{flox/flox}$ mice. We also thank Mr. Joshua R. Jefferson's work on the tissue processing and histology in our department.

Abbreviations

2-DG	2-deoxyglucose
3PO	3-(3-Pyridinyl)-1-(4-pyridinyl)-2-propen-1-one
Ang-1	Angiopoietin-1
CFR	Coronary flow reserve
DHE	Dihydroethidium
ECAR	Extracellular acidification rate
DMSO	Dimethyl sulfoxide
ECKO	Endothelial-specific SIRT3 knockout
ECM	Extracellular basement membrane matrix
ET	Ejection fraction
HIF	Hypoxia-inducible factor

HFpEF	Heart failure with preserved ejection fraction
HFrEF	Heart failure with reduced ejection fraction
IB4	Isolectin B4
IVRT	Isovolumic relaxation time
IVCT	Isovolumic contraction time
LCA	Left proximal coronary artery
LV	Left ventricle
MPI	Myocardial performance index
PFKFB3	6-phosphofructo-2-kinase/fructose-2, 6-bisphosphatase isoform 3
PW Doppler	Pulsed-wave Doppler
ROS	Reactive oxygen species
SIRT3	Sirtuin3
VEGF	Vascular endothelial growth factor
vWF	von Willebrand factor
WT	Wild-type

References

1. Brouwers FP, de Boer RA, van der Harst P, Voors AA, Gansevoort RT, Bakker SJ, et al. Incidence and epidemiology of new onset heart failure with preserved vs. reduced ejection fraction in a community-based cohort: 11-year follow-up of PREVEND. Eur Heart J. 2013; 34:1424–31. [PubMed: 23470495]
2. Lam CS, Donal E, Kraigher-Krainer E, Vasan RS. Epidemiology and clinical course of heart failure with preserved ejection fraction. Eur J Heart Fail. 2011; 13:18–28. [PubMed: 20685685]
3. Mohammed SF, Hussain S, Mirzoyev SA, Edwards WD, Maleszewski JJ, Redfield MM. Coronary microvascular rarefaction and myocardial fibrosis in heart failure with preserved ejection fraction. Circulation. 2015; 131:550–9. [PubMed: 25552356]
4. Tanno M, Kuno A, Horio Y, Miura T. Emerging beneficial roles of sirtuins in heart failure. Basic Res Cardiol. 2012; 107:273. [PubMed: 22622703]
5. Upadhya B, Taffet GE, Cheng CP, Kitzman DW. Heart failure with preserved ejection fraction in the elderly: scope of the problem. J Mol Cell Cardiol. 2015; 83:73–87. [PubMed: 25754674]
6. Dhingra A, Garg A, Kaur S, Chopra S, Batra JS, Pandey A, et al. Epidemiology of heart failure with preserved ejection fraction. Curr Heart Fail Rep. 2014; 11:354–65. [PubMed: 25224319]
7. Andersen MJ, Borlaug BA. Heart failure with preserved ejection fraction: current understandings and challenges. Curr Cardiol Rep. 2014; 16:501. [PubMed: 24893938]
8. Borlaug BA, Olson TP, Lam CS, Flood KS, Lerman A, Johnson BD, et al. Global cardiovascular reserve dysfunction in heart failure with preserved ejection fraction. J Am Coll Cardiol. 2010; 56:845–54. [PubMed: 20813282]

9. Farrero M, Blanco I, Batlle M, Santiago E, Cardona M, Vidal B, et al. Pulmonary hypertension is related to peripheral endothelial dysfunction in heart failure with preserved ejection fraction. Circ Heart Fail. 2014; 7:791–8. [PubMed: 25047042]
10. Guarani V, Potente M. SIRT1 - a metabolic sensor that controls blood vessel growth. Curr Opin Pharmacol. 2010; 10:139–45. [PubMed: 20149740]
11. Nogueiras R, Habegger KM, Chaudhary N, Finan B, Banks AS, Dietrich MO, et al. Sirtuin 1 and sirtuin 3: physiological modulators of metabolism. Physiol Rev. 2012; 92:1479–514. [PubMed: 22811431]
12. Lanza IR, Short DK, Short KR, Raghavakaimal S, Basu R, Joyner MJ, et al. Endurance exercise as a countermeasure for aging. Diabetes. 2008; 57:2933–42. [PubMed: 18716044]
13. Zeng H, Vaka VR, He X, Booz GW, Chen JX. High-fat diet induces cardiac remodelling and dysfunction: assessment of the role played by SIRT3 loss. J Cell Mol Med. 2015; 19:1847–56. [PubMed: 25782072]
14. Hou X, Zeng H, He X, Chen JX. Sirt3 is essential for apelin-induced angiogenesis in post-myocardial infarction of diabetes. J Cell Mol Med. 2015; 19:53–61. [PubMed: 25311234]
15. De BK, Georgiadou M, Schoors S, Kuchnio A, Wong BW, Cantelmo AR, et al. Role of PFKFB3-driven glycolysis in vessel sprouting. Cell. 2013; 154:651–63. [PubMed: 23911327]
16. Goveia J, Stapor P, Carmeliet P. Principles of targeting endothelial cell metabolism to treat angiogenesis and endothelial cell dysfunction in disease. EMBO Mol Med. 2014; 6:1105–20. [PubMed: 25063693]
17. Schoors S, De BK, Cantelmo AR, Georgiadou M, Ghesquiere B, Cauwenberghs S, et al. Partial and transient reduction of glycolysis by PFKFB3 blockade reduces pathological angiogenesis. Cell Metab. 2014; 19:37–48. [PubMed: 24332967]
18. Xu Y, An X, Guo X, Habtetsion TG, Wang Y, Xu X, et al. Endothelial PFKFB3 plays a critical role in angiogenesis. Arterioscler Thromb Vasc Biol. 2014; 34:1231–9. [PubMed: 24700124]
19. He X, Zeng H, Chen JX. Ablation of SIRT3 causes coronary microvascular dysfunction and impairs cardiac recovery post myocardial ischemia. Int J Cardiol. 2016; 215:349–57. [PubMed: 27128560]
20. Gao S, Ho D, Vatner DE, Vatner SF. Echocardiography in Mice. Curr Protoc Mouse Biol. 2011; 1:71–83. [PubMed: 21743841]
21. Tao YK, Zeng H, Zhang GQ, Chen ST, Xie XJ, He X, et al. Notch3 deficiency impairs coronary microvascular maturation and reduces cardiac recovery after myocardial ischemia. Int J Cardiol. 2017; 236:413–22. [PubMed: 28131704]
22. Pozzi A, Moberg PE, Miles LA, Wagner S, Soloway P, Gardner HA. Elevated matrix metalloprotease and angiostatin levels in integrin alpha 1 knockout mice cause reduced tumor vascularization. Proc Natl Acad Sci U S A. 2000; 97:2202–7. [PubMed: 10681423]
23. Clem B, Telang S, Clem A, Yalcin A, Meier J, Simmons A, et al. Small-molecule inhibition of 6-phosphofructo-2-kinase activity suppresses glycolytic flux and tumor growth. Mol Cancer Ther. 2008; 7:110–20. [PubMed: 18202014]
24. Chen JX, Meyrick B. Hypoxia increases Hsp90 binding to eNOS via PI3K-Akt in porcine coronary artery endothelium. Lab Invest. 2004; 84:182–90. [PubMed: 14661033]
25. Justus CR, Leffler N, Ruiz-Echevarria M, Yang LV. In vitro cell migration and invasion assays. J Vis Exp. 2014
26. Chen JX, Lawrence ML, Cunningham G, Christman BW, Meyrick B. HSP90 and Akt modulate Ang-1-induced angiogenesis via NO in coronary artery endothelium. J Appl Physiol (1985). 2004; 96:612–20. [PubMed: 14555685]
27. Zeng H, He X, Hou X, Li L, Chen JX. Apelin gene therapy increases myocardial vascular density and ameliorates diabetic cardiomyopathy via upregulation of sirtuin 3. Am J Physiol Heart Circ Physiol. 2014; 306:H585–H597. [PubMed: 24363305]
28. Chen JX, Stinnett A. Disruption of Ang -1/Tie-2 signaling contributes to the impaired myocardial vascular maturation and angiogenesis in type II diabetic mice. Arterioscler Thromb Vasc Biol. 2008; 28:1606–13. [PubMed: 18556567]

29. Chen JX, Zeng H, Tuo QH, Yu H, Meyrick B, Aschner JL. NADPH oxidase modulates myocardial Akt, ERK1/2 activation, and angiogenesis after hypoxia-reoxygenation. Am J Physiol Heart Circ Physiol. 2007; 292:H1664–H1674. [PubMed: 17220182]
30. Chen JX, Zeng H, Lawrence ML, Blackwell TS, Meyrick B. Angiopoietin-1-induced angiogenesis is modulated by endothelial NADPH oxidase. Am J Physiol Heart Circ Physiol. 2006; 291:H1563–H1572. [PubMed: 16679392]
31. Cai H, Dikalov S, Griendling KK, Harrison DG. Detection of reactive oxygen species and nitric oxide in vascular cells and tissues: comparison of sensitivity and specificity. Methods Mol Med. 2007; 139:293–311. [PubMed: 18287681]
32. Fernandez-Marcos PJ, Jeninga EH, Canto C, Harach T, de Boer VC, Andreux P, et al. Muscle or liver-specific Sirt3 deficiency induces hyperacetylation of mitochondrial proteins without affecting global metabolic homeostasis. Sci Rep. 2012; 2:425. [PubMed: 22645641]
33. Dittenhafer-Reed KE, Richards AL, Fan J, Smallegan MJ, Fotuhi SA, Kemmerer ZA, et al. SIRT3 mediates multi-tissue coupling for metabolic fuel switching. Cell Metab. 2015; 21:637–46. [PubMed: 25863253]
34. Jing E, Emanuelli B, Hirschey MD, Boucher J, Lee KY, Lombard D, et al. Sirtuin-3 (Sirt3) regulates skeletal muscle metabolism and insulin signaling via altered mitochondrial oxidation and reactive oxygen species production. Proc Natl Acad Sci U S A. 2011; 108:14608–13. [PubMed: 21873205]
35. Li H, Feng Z, Wu W, Li J, Zhang J, Xia T. SIRT3 regulates cell proliferation and apoptosis related to energy metabolism in non-small cell lung cancer cells through deacetylation of NMNAT2. Int J Oncol. 2013; 43:1420–30. [PubMed: 24042441]
36. Koentges C, Pfeil K, Schnick T, Wiese S, Dahlbock R, Cimolai MC, et al. SIRT3 deficiency impairs mitochondrial and contractile function in the heart. Basic Res Cardiol. 2015; 110:36. [PubMed: 25962702]
37. Vallerie SN, Bornfeldt KE. Metabolic Flexibility and Dysfunction in Cardiovascular Cells. Arterioscler Thromb Vasc Biol. 2015; 35:e37–e42. [PubMed: 26310811]
38. Eelen G, de ZP, Simons M, Carmeliet P. Endothelial cell metabolism in normal and diseased vasculature. Circ Res. 2015; 116:1231–44. [PubMed: 25814684]
39. Wan A, Rodrigues B. Endothelial cell-cardiomyocyte crosstalk in diabetic cardiomyopathy. Cardiovasc Res. 2016; 111:172–83. [PubMed: 27288009]
40. Fraisl P, Mazzone M, Schmidt T, Carmeliet P. Regulation of angiogenesis by oxygen and metabolism. Dev Cell. 2009; 16:167–79. [PubMed: 19217420]
41. Minchenko O, Opentanova I, Caro J. Hypoxic regulation of the 6-phosphofructo-2-kinase/fructose-2,6-bisphosphatase gene family (PFKFB-1–4) expression in vivo. FEBS Lett. 2003; 554:264–70. [PubMed: 14623077]
42. Obach M, Navarro-Sabate A, Caro J, Kong X, Duran J, Gomez M, et al. 6-Phosphofructo-2-kinase (pfkfb3) gene promoter contains hypoxia-inducible factor-1 binding sites necessary for transactivation in response to hypoxia. J Biol Chem. 2004; 279:53562–70. [PubMed: 15466858]
43. Scortegagna M, Ding K, Oktay Y, Gaur A, Thurmond F, Yan LJ, et al. Multiple organ pathology, metabolic abnormalities and impaired homeostasis of reactive oxygen species in Epas1−/− mice. Nat Genet. 2003; 35:331–40. [PubMed: 14608355]
44. Liu H, Chen T, Li N, Wang S, Bu P. Role of SIRT3 in Angiotensin II-induced human umbilical vein endothelial cells dysfunction. BMC Cardiovasc Disord. 2015; 15:81. [PubMed: 26223796]

Highlights

- SIRT3 deletion shifts ECs from glycolytic metabolism to mitochondrial respiration.
- SIRT3 loss results in EC dysfunction via impaired glycolysis and PFKFB3 signaling.
- Mice lacking EC SIRT3 develop microvascular dysfunction and diastolic dysfunction.

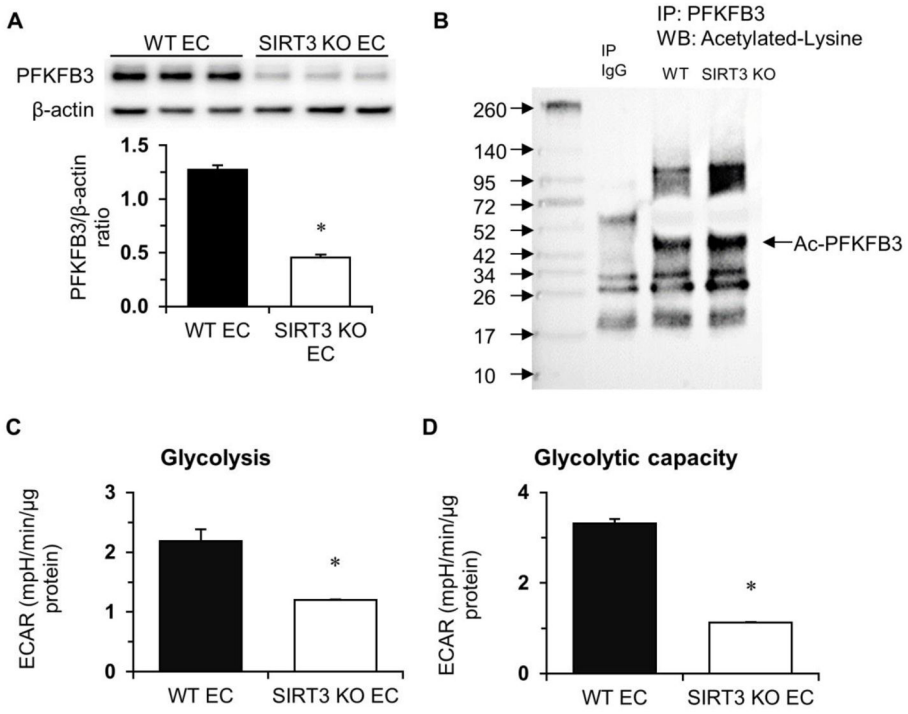

Figure 1. Endothelial SIRT3 deletion alters EC glycolytic metabolism

A, Immunoblot of glycolytic enzyme-PFKFB3 shows decreased expression of PFKFB3 in SIRT3 KO-ECs. **B,** Acetylation of PFKFB3 is increased in SIRT3 KO-ECs compared to WT-ECs. **C and D,** Glycolysis data are calculated and expressed as extracellular acidification rate (ECAR). Glycolysis and glycolytic capacity are significantly decreased in SIRT3 KO-ECs. (n=3 per group; *p<0.05 *vs.* WT-ECs).

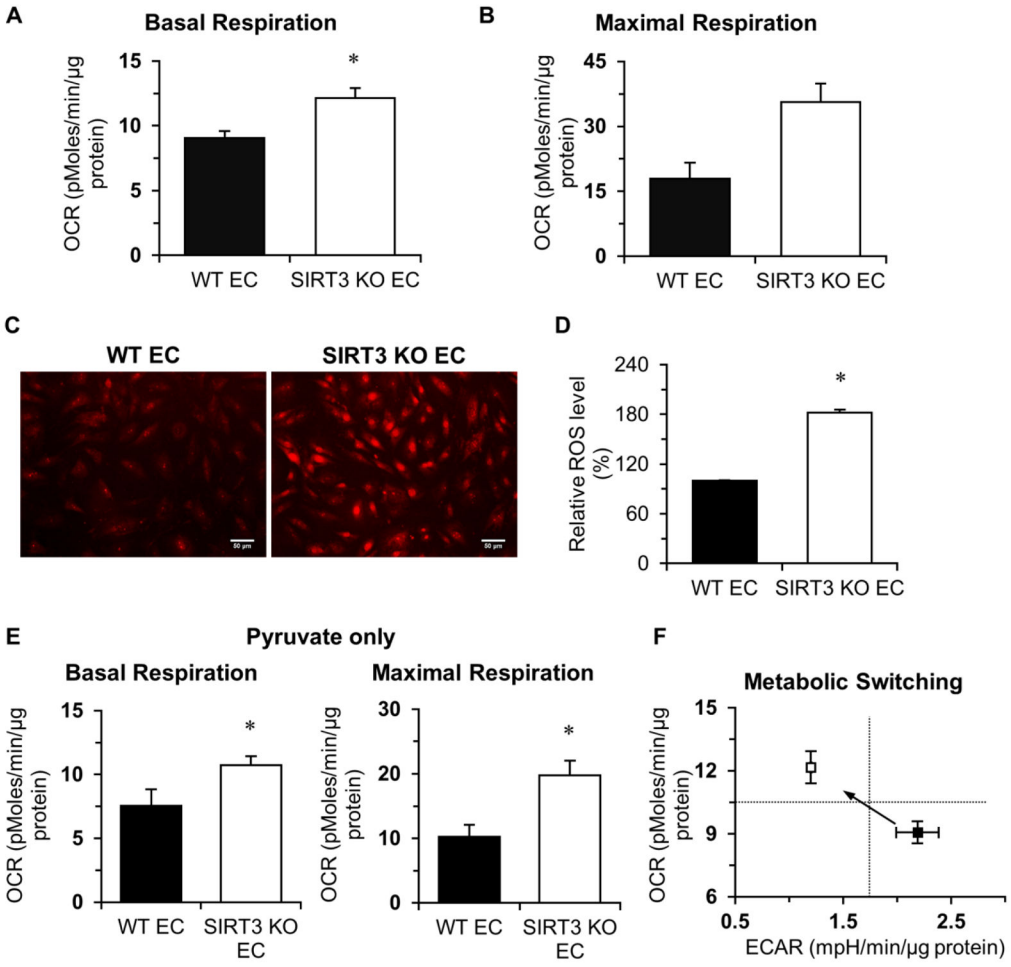

Figure 2. Endothelial SIRT3 deletion increases oxygen consumption rate

A and B, Basal oxygen consumption rate (OCR) and maximal respiration are dramatically increased in SIRT3 KO-ECs. **C and D,** DHE staining indicates that the production of superoxide was significantly increased in SIRT3 KO-ECs. **E,** The basal OCR and maximal respiration are also significantly increased when only pyruvate (1 mM) was present in the assay medium. **F,** Loss of endothelial SIRT3 results in a metabolic shift from oxygen-independent glycolysis to oxygen-dependent oxidative phosphorylation. (n=3 per group; *p<0.05 *vs.* WT-ECs).

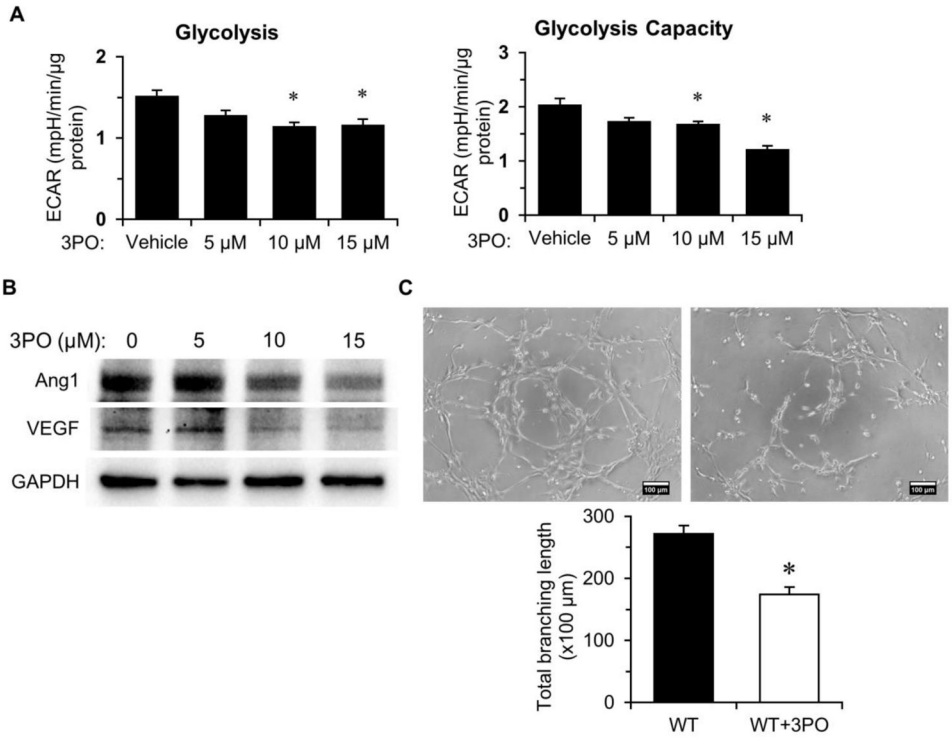

Figure 3. PFKFB3 inhibition alters glycolysis and angiogenesis in ECs

A, Treatment with PFKFB3 inhibitor, 3PO, results in decline of glycolysis and glycolytic capacity in ECs in a dose-dependent manner. (n=3 per group; *p<0.05 vs. vehicle). **B,** Immunoblotting analysis indicates that treatment with 3PO results in decreased expression of Ang1 and VEGF. **C,** ECs were treated with 10 µM of 3PO for 24 hours, then tube formation was assessed using a Matrigel assay. Images represent WT and SIRT3 KO-EC network formation at 6 hours of incubation. Quantifications of EC network formation reveals a significant decrease in total branching length in 3PO -treated WT-ECs versus Vehicle-treated WT-ECs. (n=3 per group; *p<0.05 *vs.* WT-ECs).

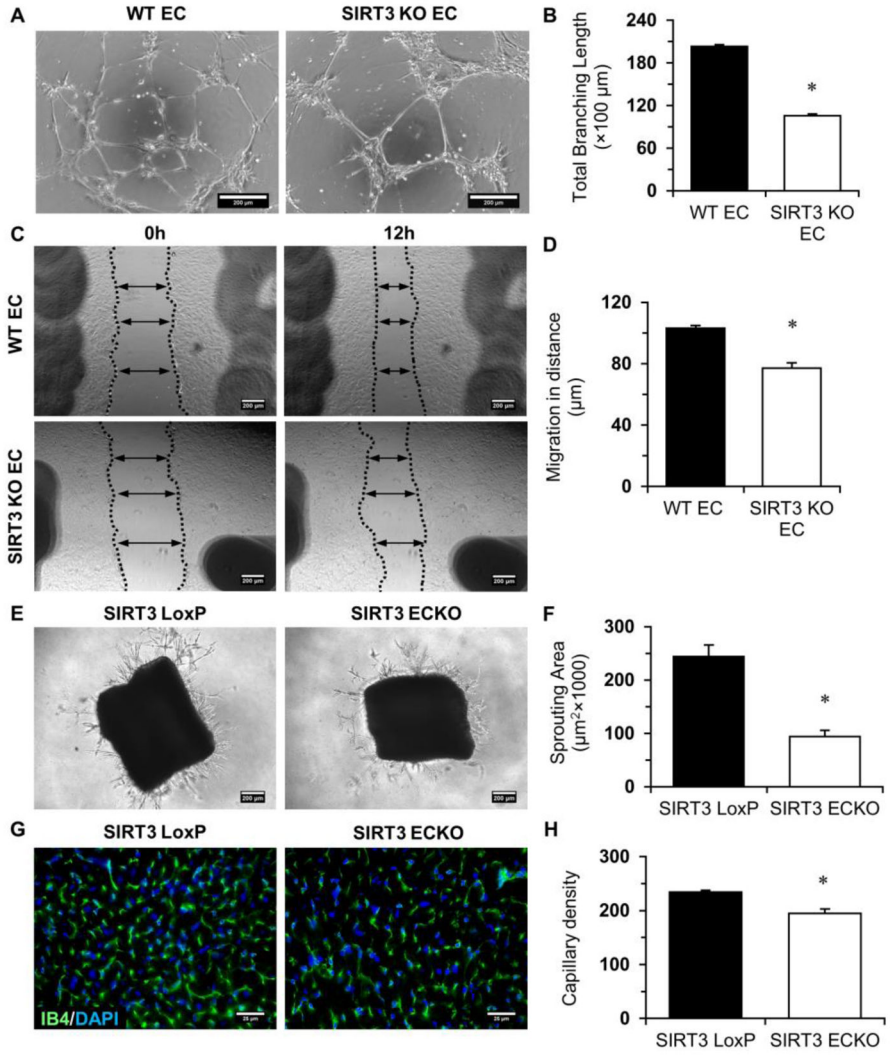

Figure 4. SIRT3 deletion impairs endothelial angiogenic properties

A and B, EC tube formation was assessed using a Matrigel assay. Images represent WT and SIRT3 KO-EC network formation at 6 hours of incubation. Quantifications of EC network formation reveals a significant decrease in total branching length for SIRT3 KO-ECs versus WT-ECs. **C and D,** Migration of WT-ECs and SIRT3 KO-ECs was assessed using a scratch wound assay. Migration in distance is significantly decreased for SIRT3 KO-ECs 12 hours after scratch. (n=3; *p<0.05 *vs.* WT-ECs). **E and F,** The aortas from SIRT3 LoxP and SIRT3 ECKO mice were embedded into ECM gel and cultured for 7 days. The sprouting area is significantly decreased in SIRT3 ECKO aortas. (n=3; *p<0.05 *vs.* SIRT3 LoxP). **G and H,** IB4 staining (green) and quantification presented as the number of vessels per field indicates that the capillary density in the LV myocardium of the SIRT3 ECKO mice is significantly decreased when compared to SIRT3 LoxP mice. (n=4–5; *p<0.05 *vs.* SIRT3 LoxP).

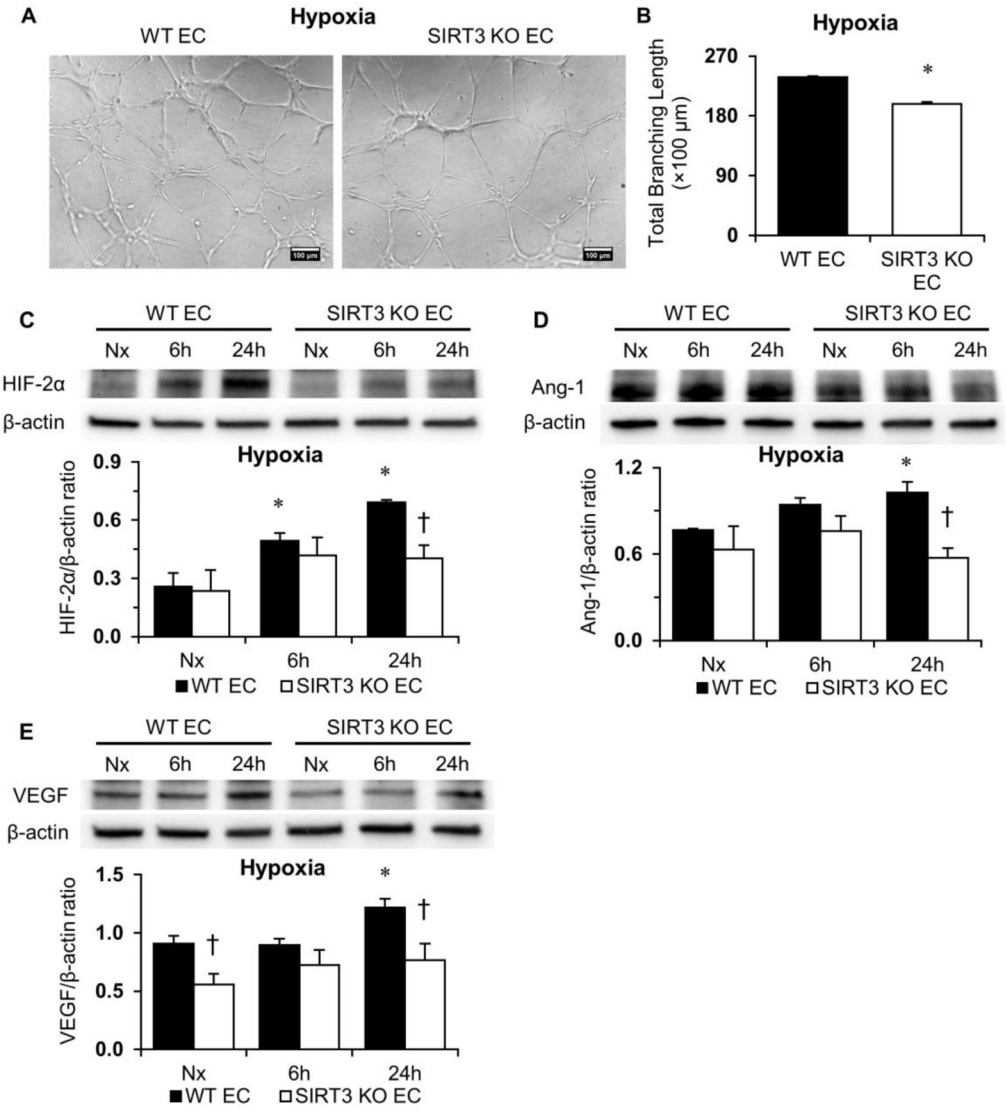

Figure 5. SIRT3 deletion impairs hypoxia signaling

A and B, WT and SIRT3 KO-ECs were incubated under hypoxia for 6 hours. EC tube formation is significantly decreased in SIRT3 KO-ECs while exposed to hypoxia for 6 hours. (n=3; *p<0.05 vs. WT-ECs). **C–E,** Expression of HIF-2α is significantly lower in SIRT3 KO-ECs after exposure to hypoxia for 24 hours. Moreover, hypoxia-induced expressions of Ang-1 and VEGF are also significantly lower in SIRT3 KO-ECs after exposure to hypoxia for 24 hours. (n=3; *p<0.05 *vs.* Nx (normoxia); †p<0.05 *vs.* WT-ECs).

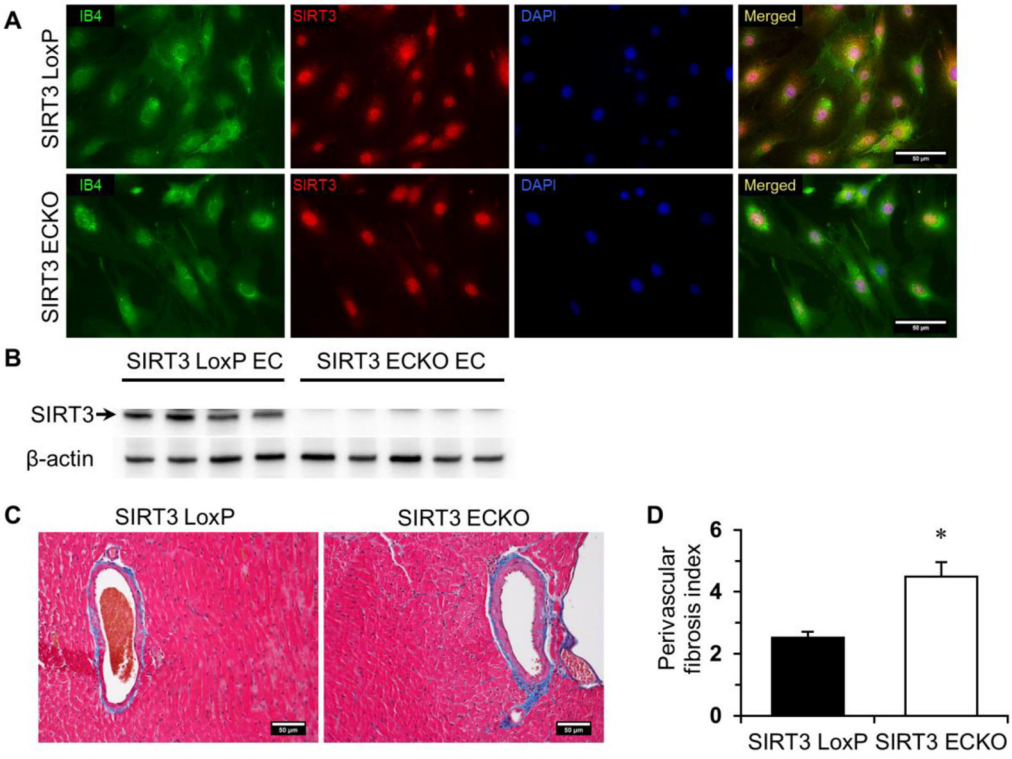

Figure 6. Endothelial specific ablation of SIRT3 increases perivascular fibrosis

A, Isolated endothelial cells from SIRT3 LoxP or SIRT3 ECKO mice were co-stained with rabbit anti-SIRT3 antibody (red) and IB4 (green). The representative images show that SIRT3 is not detected in the cytosolic compartment of ECs from SIRT3 ECKO mice. **B,** The absence of SIRT3 was also confirmed by immunoblot analysis. **C and D,** Semi-quantification of Masson's trichrome staining indicates that perivascular fibrosis is significantly increased in the heart of SIRT3 ECKO mice. (n=4–5; *$p < 0.05$ vs. SIRT3 LoxP).

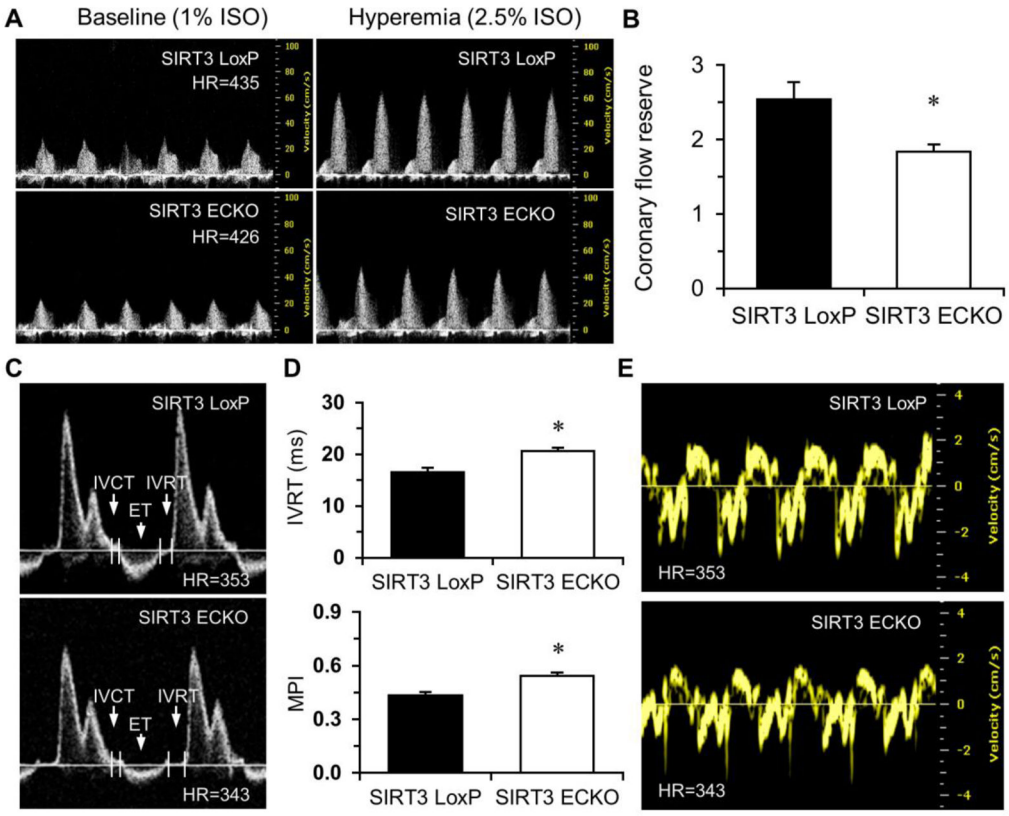

Figure 7. Endothelial specific ablation of SIRT3 reduces coronary flow reserve (CFR) and impairs diastolic function

A and B, Representative images of Pulsed-wave (PW) Doppler of LCA at baseline or under hyperemic conditions induced by inhalation of 1% or 2.5% isoflurane, respectively. Coronary flow reserve is calculated as the ratio of hyperemic peak diastolic flow velocity to baseline peak diastolic flow velocity. There is a significant decrease in CFR in SIRT3 ECKO mice compared to SIRT3 LoxP mice. (n=5; *p < 0.05 vs. SIRT3 LoxP). **C and D,** Transmitral inflow Doppler reveals that isovolumic relaxation time (IVRT) is prolonged in SIRT3 ECKO mice compared to SIRT3 LoxP mice. Myocardial performance index (MPI) is significantly increased in SIRT3 ECKO mice *vs.* SIRT3 LoxP mice. (n=9–12; *p < 0.05 vs. SIRT3 LoxP). **E,** Representative images of Tissue Doppler of mitral annulus motion of SIRT3 LoxP and SIRT3 ECKO mice.

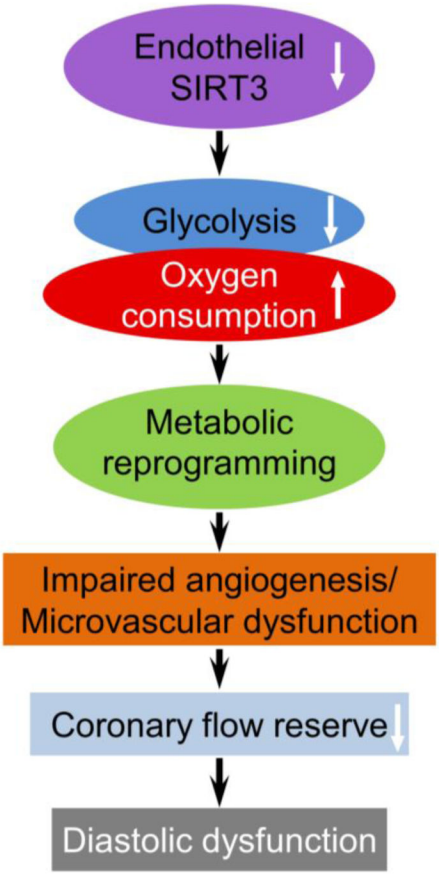

Figure 8. Schematic of the proposed role of SIRT3 in diastolic function

Loss of SIRT3 in EC reprograms endothelial metabolism which impairs angiogenesis and microvascular function and eventually leads to diastolic dysfunction.

Table 1

Assessment of diastolic function in SIRT3 LoxP and SIRT3 ECKO mice

Diastolic index	SIRT3 LoxP (n=9)	SIRT3 ECKO (n=12)
E (cm/s)	78.24 ± 2.84	77.97 ± 1.21
A (cm/s)	45.45 ± 1.95	46.96 ± 1.77
E/A	1.74 ± 0.08	1.69 ± 0.06
E′ (cm/s)	2.62 ± 0.12	2.24 ± 0.09 *
A′ (cm/s)	2.27 ± 0.13	2.05 ± 0.07
E/E′	30.24 ± 1.38	35.33 ± 1.28 *

* $p < 0.05$ *vs.* SIRT3 LoxP mice.